Toward a Fundamental Understanding of Molecular Recognition: A Synthetic and Computational Study of Morphological Control of $Ca_3Al_2(OH)_{12}$

Andrew M. Fogg,* Amal J. Freij, Andrew L. Rohl, Mark I. Ogden, and Gordon M. Parkinson

A. J. Parker Cooperative Research Centre for Hydrometallurgy, School of Applied Chemistry, Curtin University of Technology, P.O. Box U1987, Perth 6845, Australia

Received: August 27, 2001; In Final Form: April 9, 2002

Molecular modeling has been used to predict both the structure and morphology of $Ca_3Al_2(OH)_{12}$. The calculated structure is in excellent agreement with the experimentally determined one with a less than 1% decrease in the lattice parameter. The morphology of $Ca_3Al_2(OH)_{12}$ was predicted to be the 24-sided deltoidal icositetrahedron formed from the {112} face, and while the experimental morphology of $Ca_3Al_2(OH)_{12}$ is generally poorly defined, the smaller crystals in the sample did display this morphology. This experimental morphology of $Ca_3Al_2(OH)_{12}$ has been shown to be strongly dependent on the presence of crystal growth modifier anions in the reaction solution with each additive studied favoring a specific crystal face to the exclusion of all others. It was found that sulfate stabilizes the {111} face, leading to the formation of crystals with an octahedral morphology, oxalate favors the {110} face, forming rhombic dodecahedral crystals, and EDTA interacts preferentially with the {210} face, generating crystals with a tetrakis hexahedral morphology. These experimental observations have been explained by molecular modeling, which demonstrated that the lowest replacement energy for each of the additive anions was for the experimentally observed crystal face.

Molecular recognition refers to the selective binding of a molecule or ion to a complementary host.[1] These interactions have frequently been employed to control crystallization and mineralization processes but with little understanding of their mode of action.[2,3] For example, the synthesis of microporous and mesoporous materials is strongly dependent on the templating molecule used,[4] surfactant monolayers can be used to selectively nucleate inorganic materials,[5] and skeletal structures mimicking those observed in nature can be prepared by careful control of the crystallizing medium.[6]

For molecular crystals, morphological modification had been brought about by the use of stereospecific inhibition of the growth of particular crystal faces.[2,3] In inorganic systems, however, such a strategy is not generally applicable and a more empirical approach exploiting the bonding and packing in the crystal structure must be used. In this way, it has proved possible to introduce crystal faces into the morphology of materials such as $CaCO_3$,[7] KNO_3,[8] and K_2SO_4,[9] which are not normally observed. In other cases, it has proved possible for the morphology to be completely altered such that it comprises a single crystal face that is not originally observed. For example, growth of NaCl in the presence of urea leads to the formation of octahedral crystals ({111} face) rather than the usual cubic morphology ({100} face).[10]

Computational techniques have become a powerful and widely used tool for studying the solid-state structures of organic,[11] biological,[12] polymeric,[13] and inorganic systems.[14] Lattice energy optimization, where a minimum energy periodic structure is obtained from a starting configuration using a well-defined potential set, is particularly applicable to inorganic structures. The methodologies and applications of modeling techniques have recently been reviewed by Catlow et al.[15]

One important application of these atomistic modeling techniques is to predict the morphology and determine the surface configuration of both organic and inorganic crystals. In this way, it has proved possible to predict the experimental morphologies of materials as diverse as gibbsite (γ-$Al(OH)_3$)[16] and α-lactose monohydrate.[17] In another study, the appearance of new crystal faces in the experimental morphology of calcite grown in the presence of lithium and magnesium cations was able to be predicted by atomistic simulation.[7] These techniques have also been used to explain the action of inhibitors on crystal growth[18,19] and to investigate the effect of hydration on crystal surfaces.[20,21]

$Ca_3Al_2(OH)_{12}$ is the silicon free member of the garnet family of minerals, having a cubic structure in which Al is in an octahedral environment and Ca is 8-coordinate in a square antiprismatic arrangement.[22,23] It is an important constituent of cement and a byproduct of the Bayer Process.[24,25] Previous molecular modeling work on this family of minerals has centered on the calculation of the defect energy and structure in grossular, resulting from the formation of silicon vacancy defects surrounded by four hydroxide groups, although no simulation of $Ca_3Al_2(OH)_{12}$ was performed.[26] In this work the effects of crystal growth modifiers on $Ca_3Al_2(OH)_{12}$ will be examined from both an experimental and computational viewpoint. Probing the responses of a single crystal system toward molecules in this way will allow for a fuller understanding of the factors that lead to molecular recognition in these systems.

Experimental Details

Synthesis of $Ca_3Al_2(OH)_{12}$. The synthesis of $Ca_3Al_2(OH)_{12}$ was based on the method described previously by Whittington.[27] In a typical experiment, 6.44 g of gibbsite (γ-$Al(OH)_3$) was dissolved in 10 mL of 13.3 M NaOH solution at 95 °C. 3.47 g of $Ca(OH)_2$, slurried in 40 mL of de-ionized water, was then added to the original solution and maintained at 95 °C for 24 h. For the reactions in the presence of either Na_2SO_4, $Na_2C_2O_4$, or Na_2EDTA the additive was added to the slurried $Ca(OH)_2$ at

10.1021/jp015528k CCC: $22.00
Published on Web 05/16/2002

a concentration of 0.035 mol/L with respect to the final solution. Powder XRD patterns of the products were recorded on a Philips PW3020 diffractometer using Cu Kα radiation and showed them to be $Ca_3Al_2(OH)_{12}$ with a small amount of residual $Ca(OH)_2$ in each case. The morphology of the samples was investigated by SEM on a Philips XL30 instrument.

Computational Method. The unit cell of $Ca_3Al_2(OH)_{12}$ was simulated using the General Utility Lattice Program (GULP)[28] using the potential model derived for hydroxides including gibbsite (γ-$Al(OH)_3$) and $Ca(OH)_2$[16] with a slight refinement of the Al−O Buckingham potential. This adjustment of the Al−O Buckingham potential was necessary to account for the differences resulting from the presence of discrete $Al(OH)_6^{3-}$ units in $Ca_3Al_2(OH)_{12}$ compared with the bridging hydroxides in $Al(OH)_3$ and led to a new *A* parameter of 1232.69 eV rather than the value of 1342.86 eV derived for gibbsite. The Dick−Overhauser shell model was used to model the polarization of the oxygen atoms in the lattice.[29] Surface calculations using this potential set were performed using the MARVIN code[30] on the following low index faces of $Ca_3Al_2(OH)_{12}$ {112}, {110}, {321}, {100}, {210}, {332}, and {111}. The methodologies used in these surface relaxation calculations and to generate the predicted morphologies have been comprehensively described elsewhere.[16,19] In $Ca_3Al_2(OH)_{12}$, it might be expected that the surface aluminum species are the same as those in the bulk, namely $Al(OH)_6^{3-}$. However, applying this condition always leads to the generated surface having a dipole moment perpendicular to it, which is unstable. Furthermore, it is evident that little or no $Al(OH)_6^{3-}$ exists in the solution.[31] Thus we have generated our surfaces by just stipulating that hydroxide bonds cannot be broken and the generated surfaces must have no perpendicular dipole. This leads to surfaces with primarily 4- and 5-coordinate surface aluminum atoms, similar to the work on gibbsite surfaces in ref 16. Note that this methodology leads to some free hydroxide on the surface. In the case of (222), one surface aluminum was 3-coordinate, which will not occur in basic solution, and thus one of the free hydroxide ions was moved into its coordination shell. For a given crystal face, several cleavage planes are possible and each one was relaxed in MARVIN.

For each face, the most stable cut was taken as being the one with the lowest surface energy and these were used in the subsequent morphology and additive calculations. Images of the solvent accessible surfaces were generated by probing the relaxed surface with a sphere of radius 1.4 Å within the Cerius[2] software suite[32] and are color coded according to the nearest atom. The potential models for sulfate[19] and oxalate[33] were taken from previous studies while those for $EDTA^{4-}$ were derived from the CVFF force field[32] and are reported in Table 1. The additive−surface interactions are described by Lennard-Jones potentials of the form $C_9r^{-9}-C_6r^{-6}$ derived from the ESFF force field.[34] These anions were then docked onto each relaxed surface in turn with the removal of an appropriate number of $Al(OH)_4^-$ and/or $Al(OH)_5^{2-}$ anions in order to maintain charge neutrality. For each face/additive combination, two different configurations were tried: (i) docking a single additive onto the surface and (ii) removing all aluminum species from the surface and docking enough additive anions to balance the charge. Following the relaxation of these surface/additive combinations by MARVIN, the replacement energy for the surface was calculated in a manner based on that used previously by Rohl et al.[19] according to the formula

$$\text{replacement energy} = (E_{S+Ad} + E_{Al}) - (E_{S+Al} + E_{Ad})$$

TABLE 1: Intramolecular Potentials Used To Describe $EDTA^{4-}$ Derived from the CVFF Force Field[a]

(i) Harmonic: $^1/_2k_2(r - r_0)$

interaction	k_2 (eV Å^{-2})
C_1-C_1	28.0075
C_1-N	30.9481
C_2-N	30.9481
C_2-C_3	24.5687
C_3-O	46.8649
$H-C_1$	29.5611
$H-C_2$	29.5611

(ii) Three-Body Harmonic: $V = {}^1/_2k_2(\theta - \theta_0)^2$

interaction	k_2 (eV rad^{-2})	θ_0
$O-C_3-O$	12.5841	123.0
C_2-C_3-O	5.9015	120.0
$H-C_2-C_3$	3.9154	109.5
C_3-C_2-N	4.3493	109.5
$H-C_2-N$	4.9729	109.5
C_2-N-C_2	7.4997	112.0
C_1-N-C_2	7.4997	112.0
$H-C_2-H$	3.8620	106.4
C_1-C_1-N	4.3493	109.5
$H-C_1-N$	4.9729	109.5
$H-C_1-H$	3.8620	106.4
$H-C_1-C_1$	3.8533	110.0

(iii) Torsion: $k(1 + \cos 3\phi)$

interaction	k (eV)
$C_3-C_2-N-C_1$	0.005784
$C_3-C_2-N-C_2$	0.005784
$H-C_2-N-C_2$	0.005784
$H-C_2-N-C_2$	0.005784
$C_2-N-C_1-C_1$	0.005784
C_2-N-C_1-H	0.005784
$N-C_1-C_1-H$	0.006861
$H-C_1-C_1-H$	0.006861

(iv) Out of Plane: $k(1 + \cos(n\,\text{phase}(\phi - \phi_0))$

interaction	k (eV)	n phase	ϕ_0
$O-C_3-C_2-O$	0.1968	+1	0

(v) Coulombic Charges

C_1	−0.124
C_2	−0.157
C_3	+0.436
N	−0.022
O	−0.675
H	+0.048

[a] Labeling scheme: $C_1 = -N-\mathbf{C}-\mathbf{C}-N-$; $C_2 = -O-C-\mathbf{C}-N-$; C_3 = carboxylate carbon.

where E_{S+Ad} is the energy of the relaxed surface after the additive has been docked onto it, E_{S+Al} is the energy of the relaxed pure surface, E_{Al} is the energy of the Al containing species infinitely far from the surface, and E_{Ad} is the energy of the additive molecule infinitely far from the surface.

Results and Discussion

The simulation of the cubic structure of $Ca_3Al_2(OH)_{12}$ was performed on the experimental structure reported by Lager et al.[23] It was found that there was excellent agreement between the experimental and calculated structures after minimization, with less than a 1% difference in the lattice parameter. The structural parameters are summarized in Table 2 and the calculated structure is shown in Figure 1.

The surface relaxation calculations were performed on all possible stable cuts of the following six crystal faces: {112}, {110}, {321}, {210}, {332}, and {111}. The {100} surface was

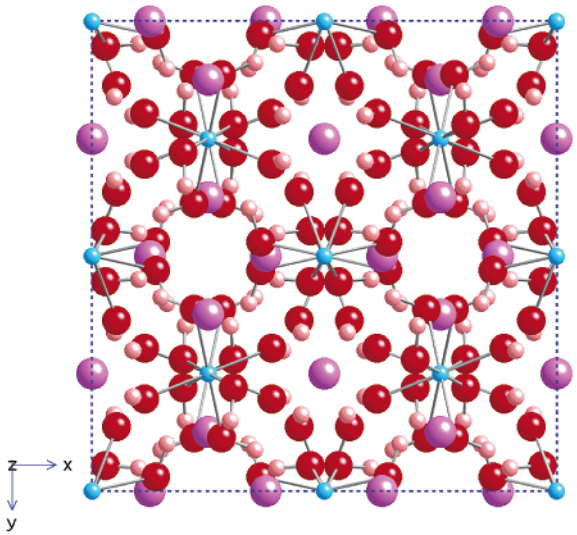

Figure 1. Calculated structure of $Ca_3Al_2(OH)_{12}$. Color key: Al, blue; Ca, purple; O, red; H, pink.

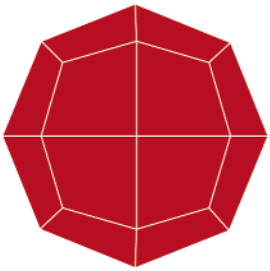

Figure 2. Predicted morphology of $Ca_3Al_2(OH)_{12}$ consisting of a 24-sided polyhedron bounded by the {112} faces.

TABLE 2: Comparison of the Observed and Calculated Structural Parameters for $Ca_3Al_2(OH)_{12}$

parameter	observed[23]	calculated	difference (%)
a (Å)	12.5695	12.5638	0.05
vol (Å^3)	1985.88	1983.19	0.14
O_x	0.0288	0.0375	−0.87
O_y	0.0522	0.0517	0.05
O_z	0.6402	0.6405	−0.03
H_x	0.1517	0.1466	0.51
H_y	0.0913	0.0782	1.31
H_z	0.7985	0.8079	−0.94

TABLE 3: Summary of the Surface and Attachment Energies and the Surface Species for the Most Stable Cut of Each Surface of $Ca_3Al_2(OH)_{12}$

surface	surface energy (J m^{-2})	attachment energy (eV mol^{-1})	surface species
(112)	0.48	−1.021	$Al(OH)_4^-$
(110)	0.70	−1.587	$Al(OH)_4^-$, $Al(OH)_5^{2-}$
(111)	0.78	−6.227	$Al(OH)_4^-$
(321)	0.64	−2.576	$Al(OH)_4^-$, $Al(OH)_5^{2-}$
(332)	0.68	−3.128	$Al(OH)_4^-$, $Al(OH)_5^{2-}$
(210)	0.59	−3.029	$Al(OH)_5^{2-}$

not examined as it is a type III surface; i.e., all possible planar cleavage planes result in a surface dipole moment.[35] The lowest relaxed surface and attachment energies for each surface are listed in Table 3 and were used to generate the relaxed growth and equilibrium morphologies for $Ca_3Al_2(OH)_{12}$, respectively. In both cases, this was the 24-sided deltoidal icositetrahedron formed from the {112} faces, which is shown in Figure 2 with a cross-section of the relaxed {112} face in Figure 3a. In general, the position of the surface cut for a given Miller index, which gives the most stable face, may differ depending on whether the relaxed surface energy or the relaxed attachment energy is used. In this system, only the high index {332} face gave different stable cuts for the two calculation methods.

The solvent accessible surfaces corresponding to the cuts with the lowest surface energy are shown in Figure 4 and on examination were found to contain $Al(OH)_4^-$ and/or $Al(OH)_5^{2-}$ species rather than the octahedral $Al(OH)_6^{3-}$ groups present in the bulk structure. This prediction of negatively charged surfaces for $Ca_3Al_2(OH)_{12}$ is consistent with an electrokinetic study that found this to be the case in basic solution.[36] The species present on each surface are summarized in Table 3. Figure 4 shows that all the surfaces are primarily constructed from hydroxyl groups as part of $Al(OH)_4^-$ or $Al(OH)_5^{2-}$ species, although calcium ions are accessible to some extent on all faces except the {211} face, which is the face predicted to be the most stable. A comparison of the geometry of the surface $Al(OH)_4^-$ and $Al(OH)_5^{2-}$ groups with their gaseous configurations optimized using the same potential model showed that there is significant distortion of those on the surfaces of $Ca_3Al_2(OH)_{12}$. For the $Al(OH)_4^-$ groups, it was found that the average Al−O bond length was 0.04 Å longer than in the gaseous configuration, though there was a variation in bond length depending on the orientation of the bond relative to the surface. The Al−O bonds, which were perpendicular to the surface, e.g., on the {112} face, were typically the same length as in the gaseous configuration, while those in the surface were notably longer. The O−Al−O bond angles in the surface aluminate groups also show a marked distortion away from the ideal tetrahedral angle of 109.5°. These distortions are generally around ±10° although a change of 14° was observed on the {111} face. The optimized gas-phase configuration for $Al(OH)_5^{2-}$ is a trigonal bipyramid with an Al−O bond length of 1.86 Å. The average lengthening of this bond in the surface species was 0.03 Å, comparable to the change in the aluminate groups. The geometry of the surface $Al(OH)_5^{2-}$ groups also shows distortions away from the idealized one with the $O_{eq}-Al-O_{eq}$ angles for the equatorial groups being changed by ±10° on average and the average axial $O_{ax}-Al-O_{ax}$ angle being 165°. These distortions presumably occur to maximize the bonding interactions at the surface and were found to be similar on all the faces examined.

Perhaps of much wider significance, this study of the surfaces of $Ca_3Al_2(OH)_{12}$ suggests that the adsorption and incorporation characteristics of the individual faces should vary widely. In a crystal growth context, the presence of differently charged species and the considerably different amounts of accessible calcium on the faces indicates that the growth of the various faces $Ca_3Al_2(OH)_{12}$ may be affected differently by the presence of impurities or additives. Also, the fact that the surface species differ from those present in the bulk structure will have significant implications for the growth mechanism.

Experimentally, the morphology of $Ca_3Al_2(OH)_{12}$ is on the whole poorly defined, resulting in no standard morphology being available for comparison with this calculated one.[27] A typical SEM image of the product from the synthesis of $Ca_3Al_2(OH)_{12}$ is shown in Figure 5a and indicates that this was also the case for the bulk of our sample. However, closer examination of the morphology of some of the smaller crystals in the sample revealed that they do have a well-defined morphology, in agreement with the one predicted by the molecular modeling study. A SEM image of these crystals is shown in Figure 5b.

Repetition of this reaction in the presence of one of Na_2SO_4, $Na_2C_2O_4$, or Na_2EDTA does, however, yield crystals with a well-defined morphology comprising a different single-crystal face, which is consistent throughout each sample. It was found

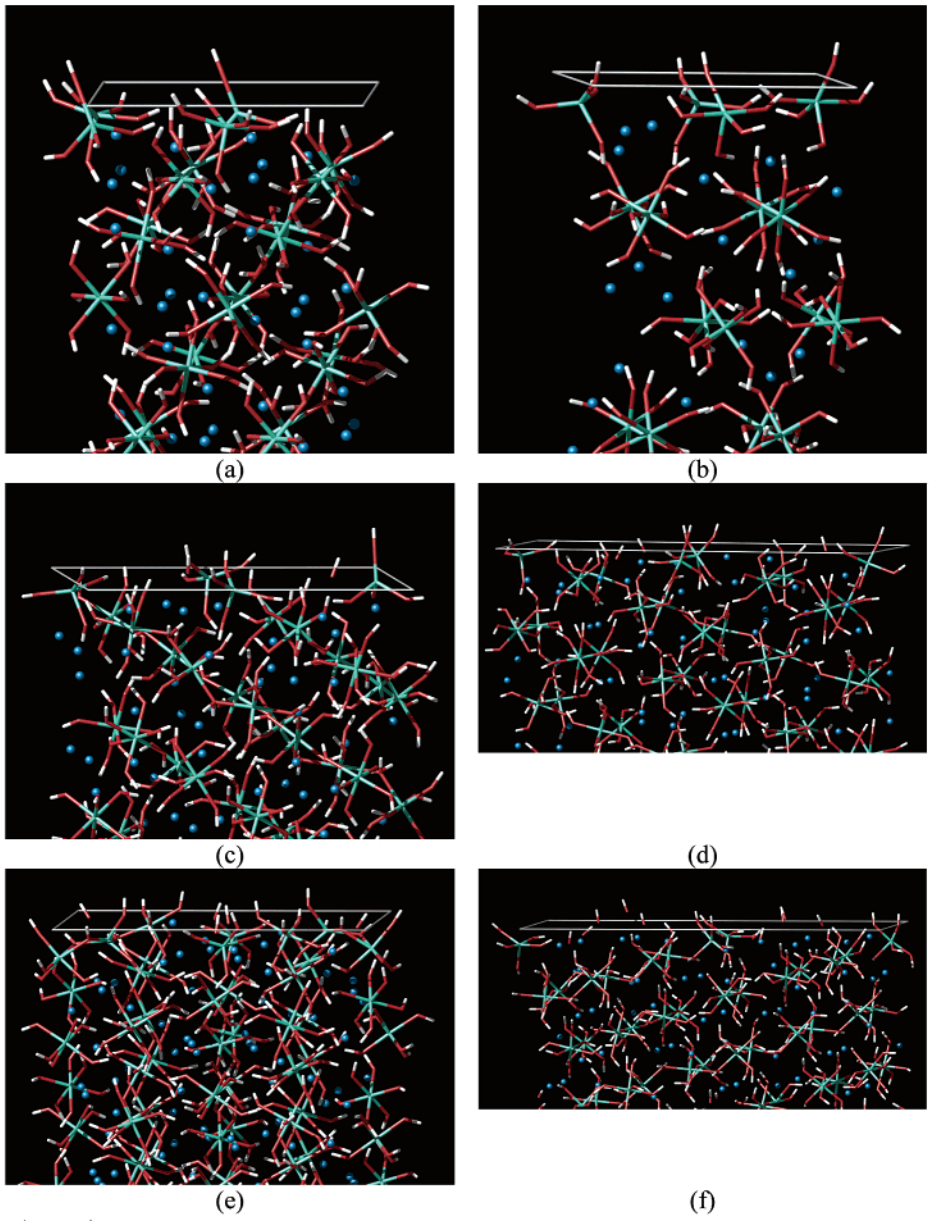

Figure 3. Cross-section of the relaxed faces: (a) (112), (b) (110), (c) (111), (d) (321), (e) (332) and (f) (210). Color key: Al, turquoise; Ca, blue; O, red; H, white.

that sulfate stabilizes the {111} face, leading to the formation of crystals with an octahedral morphology, oxalate favors the {110} face, forming rhombic dodecahedral crystals, and EDTA interacts preferentially with the {210} face, generating crystals with a tetrakis hexahedral morphology. These morphological transformations were not observed with lower concentrations of the crystal growth modifier anions. SEM images of the products of these reactions are shown in Figure 6, together with the idealized morphologies defined by the face observed in each case.

To gain an insight into the origins of this unprecedented morphological control of a single crystal system, replacement energies were calculated for the docking of sulfate, oxalate, and $EDTA^{4-}$ in turn onto each of the six relaxed crystal faces. To simplify interpretation, for each additive, the surface with the lowest replacement energy was identified, and this value was subtracted from all the other calculated replacement energies of surfaces containing the same additive. This was done separately for the docking of one anion onto the surface and for complete replacement of the surface Al species. These results are summarized in Table 4, where the most favored docking position corresponds to a relative replacement energy of zero.

From the data in Table 4, it can be seen that for replacement of all surface aluminum species, the most favorable replacement energy for each of the three crystal growth modifiers studied corresponds to the face observed experimentally in the SEM images. This, however, is not the case when a single crystal growth modifier is docked onto the surface. In these cases the most favorable replacement energy for each additive is observed for the {111} face, and while this is the face observed experimentally for sulfate, it is not seen with oxalate or EDTA. The fact that complete replacement of the surface Al species by either oxalate or EDTA is required in order to predict the experimental observations can be interpreted as being in agreement with the experimental observation that the morphological transformation with either of these crystal growth modifiers is only observed for higher anion concentrations in solution.

Examination of the relaxed surfaces containing the additive anions indicates that the anions show strong preferences for the

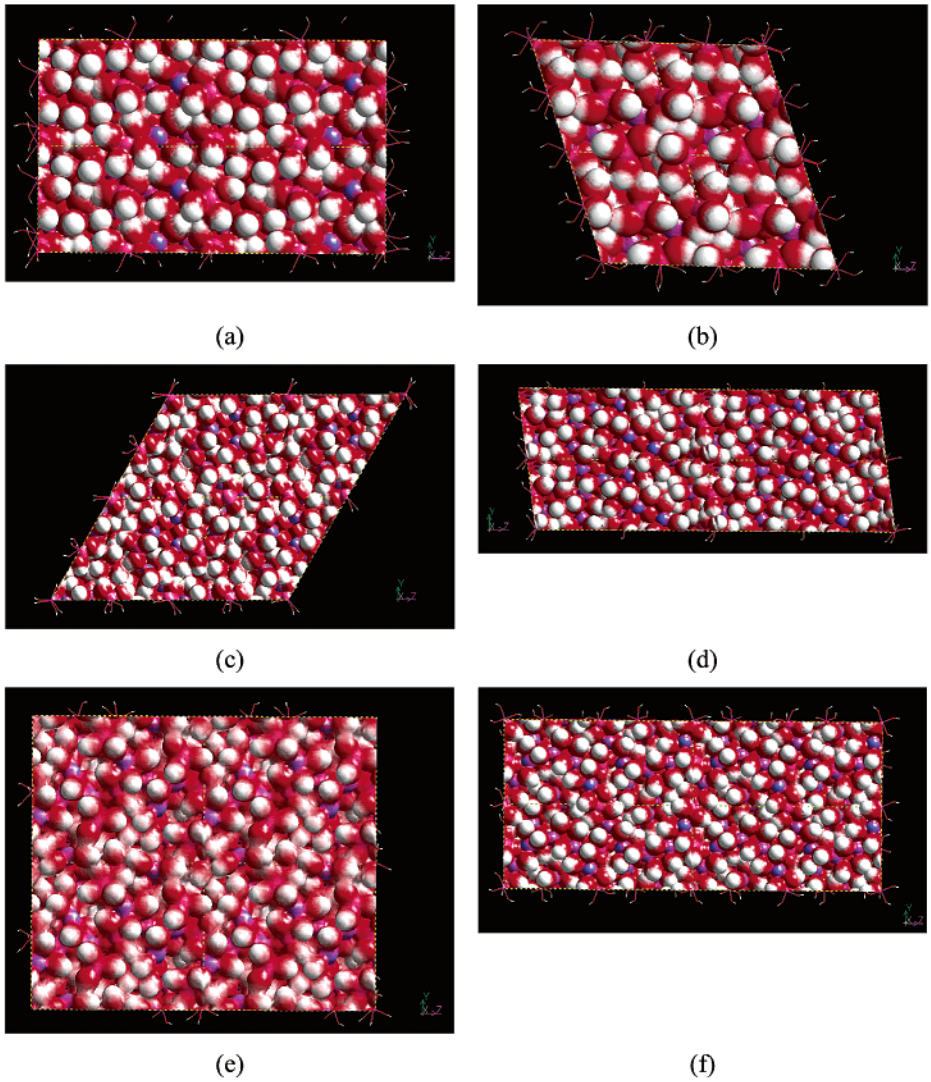

Figure 4. Solvent accessible surfaces of the relaxed surface configurations of $Ca_3Al_2(OH)_{12}$ corresponding to a probe radius of 1.4 Å color coded according to the nearest surface atom: (a) (112), (b) (110), (c) (111), (d) (321), (e) (332) and (f) (210). Color key: Al, pink; Ca, purple; O, red; H, white.

TABLE 4: Replacement Energies (kJ mol^{-1}) Relative to the Most Stable Surface for the Docking of One SO_4^{2-}, $C_2O_4^{2-}$, and $EDTA^{4-}$ Anion onto the Crystal Surfaces of $Ca_3Al_2(OH)_{12}$ and for Complete Replacement of All Surface Al Species

surface	1 × SO_4^{2-}	full SO_4^{2-}	1 × $C_2O_4^{2-}$	full $C_2O_4^{2-}$	1 × $EDTA^{4-}$	full $EDTA^{4-}$
(112)	146.2	325.5	105.9	3856.5	451.5	1978.8
(110)	61.0	107.5	103.5	0.0	77.0	1604.4
(111)	0.0	0.0	0.0	3366.9	0.0	1527.3
(321)	451.1	895.3	404.0	5559.7	979.1	231.0
(332)	604.6	1570.3	481.9	5029.1	1072.9	645.4
(210)	450.4	1685.7	404.0	7308.5	641.9	0.0

vacant aluminum sites on the surface and that there are strong interactions between the anions and the exposed Ca cations at the surface of the crystal. The relaxed surfaces containing the crystal modifiers on their preferred surface are shown in Figure 7. When the positions and orientations of the sulfate anions on the {111} surface are compared to the original $Al(OH)_4^-$ sites, it is found that there is direct replacement on half of the sites, thereby maximizing the favorable surface interactions. It is also evident that they are arranged in such a way that reflects the 3-fold symmetry of the {111} surface, creating a hexagonal array of sulfate anions over the surface. Such direct replacement is not possible for the larger oxalate and $EDTA^{4-}$ anions on the $Al(OH)_4^-$ and $Al(OH)_5^{2-}$ sites, respectively, but they still adopt positions around these sites in order to maximize the favorable interactions on the surface.

To gain an insight into the origins of the strong preferences for the individual crystal faces, it is necessary to consider the individual components of the total energy. The data in Table 4 indicate that when one additive anion is docked onto the surface, it shows a preference for the {111} face and replacement of $Al(OH)_4^-$ anions, when from purely electrostatic considerations, they would expected to occupy a vacancy created by the removal of an $Al(OH)_5^{2-}$ anion. Examination of the individual contributions to the energy shows that electrostatically the sulfate and oxalate anions favor the $Al(OH)_5^{2-}$ hole but the {111} face is found to undergo extensive surface reconstruction and the energy gained from this outweighs the reduced additive−surface interactions, resulting in the preference for the {111} face. Similarly, when the data for complete surface replacement is considered for sulfate and oxalate it is the balance between the attractive additive−surface interactions, the additive-additive repulsion, and the energy resulting from surface reconstruction that determines the preferred face. In both cases, the additive−surface interactions favor the {111} face but the anion−anion

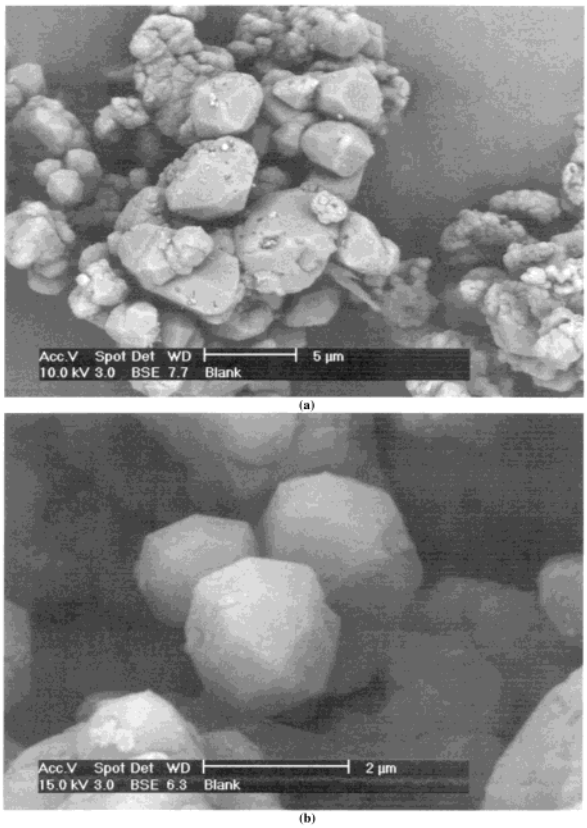

Figure 5. SEM images of (a) the bulk sample of $Ca_3Al_2(OH)_{12}$ and (b) smaller crystals of $Ca_3Al_2(OH)_{12}$ showing the deltoidal icositetrahedral morphology.

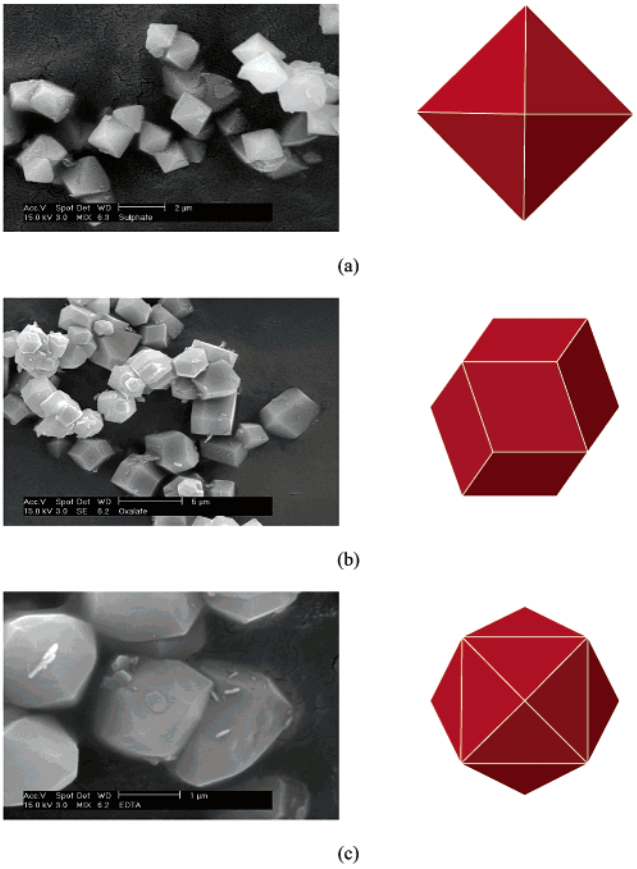

Figure 6. SEM images showing the morphology of $Ca_3Al_2(OH)_{12}$ grown in the presence of (a) sulfate, (b) oxalate, and (c) $EDTA^{4-}$ anions together with calculated morphologies defined solely by (a) {111}, (b) {110}, and (c) {210} faces.

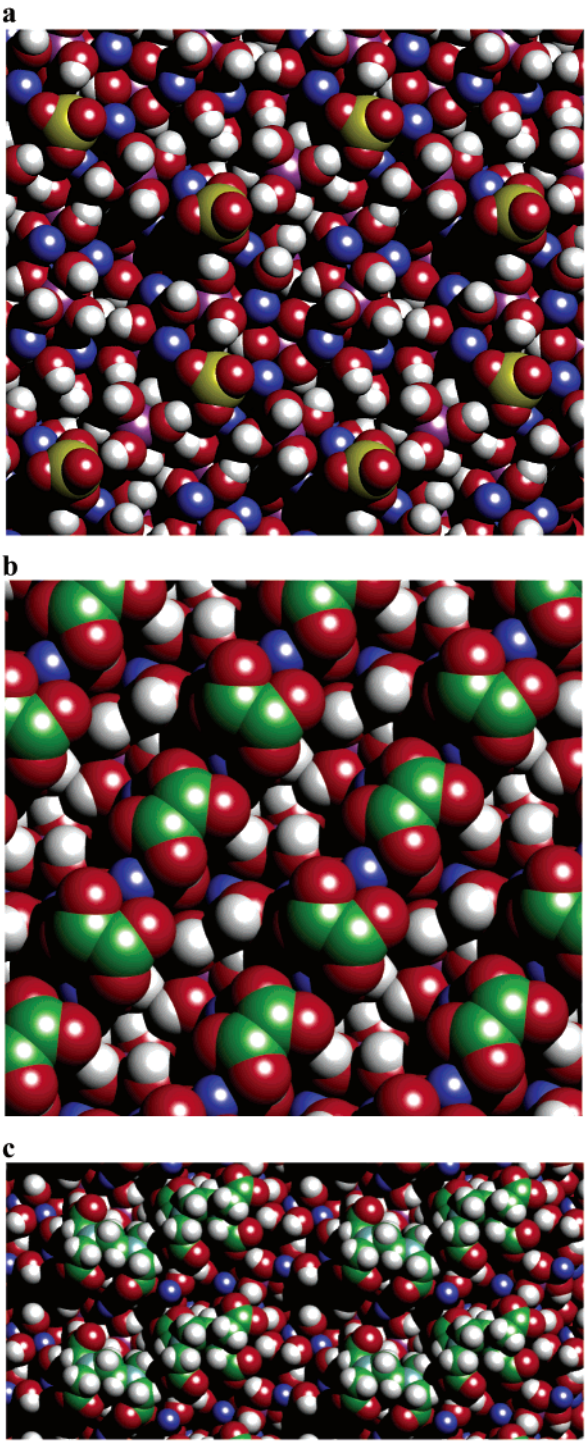

Figure 7. van der Waals surfaces of the relaxed surface/additive configurations with complete replacement of surface aluminum species: (a) sulfate on the (111) face; (b) oxalate on the (112) face; (c) $EDTA^{4-}$ on the (210) face. Color key: Al, purple; Ca, blue; O, red; H, white; S, yellow; C, green; N, gray.

interactions are much more significant for the larger oxalate anion compared to those for sulfate, leading to oxalate interacting preferentially with the {110} face where the repulsive forces are less. In the case of the $EDTA^{4-}$ anion the attractive additive−surface interactions dominate, resulting in it favoring the {210} face.

Conclusions

We have demonstrated the ability of molecular modeling to predict both the structure and morphology of $Ca_3Al_2(OH)_{12}$. The

calculated structure is in excellent agreement with the experimentally determined one, and while the majority of the sample has a poorly defined morphology, the predicted deltoidal icositetrahedral morphology is observed for smaller crystals grown in the absence of any crystal growth modifiers. Molecular modeling has also suggested that this system should be able to discriminate between different anions. Experimentally, the morphology of these crystals has been found to be strongly dependent on the presence of additives in the crystallizing solution with three different crystal growth modifiers being highly selective for three different crystal faces of $Ca_3Al_2(OH)_{12}$. This unprecedented degree of molecular recognition between the individual crystal surfaces and the additive anions leads to the transformation of the poorly defined morphology to well-defined polyhedra. The use of molecular modeling techniques to accurately predict these observations and offer an insight into their origins illustrates the potential of the technique as a predictive tool in this area.

Acknowledgment. We thank Alcoa World Alumina for financial support and Gerald Roach, Charmaine de Witt at Alcoa, and Kelly Dwyer at Curtin University for their input into this work. We also thank Julian Gale for his useful suggestions relating to this work.

References and Notes

(1) Mallouk, T. E.; Gavin, J. A. *Acc. Chem. Res.* **1998**, *31*, 209.
(2) Berkovitch-Yellin, Z.; van Mil, J.; Addadi, L.; Idelson, M.; Lahav, M.; Leiserowitz, L. *J. Am. Chem. Soc.* **1985**, *107*, 3111.
(3) Weissbuch, I.; Addadi, L.; Lahav, M.; Leiserowitz, L. *Science* **1991**, *253*, 637.
(4) Davis, M. E.; Lobo, R. F. *Chem. Mater.* **1992**, *4*, 756.
(5) Mann, S.; Heywood, B. R.; Rajam, S.; Birchall, J. D. *Nature* **1988**, *334*, 692.
(6) Walsh, D.; Mann, S. *Nature* **1995**, *377*, 320.
(7) Titiloye, J. O.; Parker, S. C.; Osguthorpe, D. J.; Mann, S. *J. Chem. Soc., Chem. Commun.* **1991**, 1494.
(8) Kipp, S.; Lacmann, R.; Rolfs, J. *J. Cryst. Growth* **1997**, *171*, 183.
(9) Bastin, L. D.; Kahr, B. *Tetrahedron* **2000**, *56*, 6633.
(10) Bunn, C. W. *Proc. Royal Soc. London A* **1933**, *141*, 567.
(11) Desiraju, G. R. *Crystal Engineering: The design of Organic Solids*; Elsevier: Amsterdam, 1989.
(12) Li, H.; Poulos, T. L. *Acta Crystallogr.* **1995**, *D51*, 21.
(13) Ferro, D. R.; Ragazzi, M.; Bruckner, S.; Meille, S. V. *Macromol. Symp.* **1995**, *89*, 529.
(14) Catlow, C. R. A.; Mackrodt, W. C. In *Lecture Notes in Physics*; Catlow, C. R. A., Mackrodt, W. C., Eds.; Springer: Berlin, 1982; p 166.
(15) Catlow, C. R. A.; Bell, R. G.; Gale, J. D. *J. Mater. Chem.* **1994**, *4*, 781.
(16) Fleming, S.; Rohl, A. L.; Lee, M.; Gale, J.; Parkinson, G. *J. Cryst. Growth* **2000**, *209*, 159.
(17) Dincer, T. D.; Parkinson, G. M.; Rohl, A. L.; Ogden, M. I. *J. Cryst. Growth* **1999**, *205*, 368.
(18) Nygren, M. A.; Gay, D. H.; Catlow, C. R. A.; Wilson, M. P.; Rohl, A. L. *J. Chem. Soc., Faraday Trans.* **1998**, *94*, 3685.
(19) Rohl, A. L.; Gay, D. H.; Davey, R. J.; Catlow, C. R. A. *J. Am. Chem. Soc.* **1996**, *118*, 642.
(20) de Leeuw, N. H.; Parker, S. C. *J. Chem. Soc., Faraday Trans.* **1997**, *93*, 467.
(21) Jones, F.; Rohl, A. L.; Farrow, J. B.; van Bronswijk, W. *Phys. Chem. Chem. Phys.* **2000**, *2*, 3209.
(22) Cohen-Addad, C.; Ducros, P.; Bertaut, E. F. *Acta Crystallogr.* **1967**, *23*, 220.
(23) Lager, G. A.; Armbruster, T.; Faber, J. *Am. Miner.* **1987**, *72*, 756.
(24) Turriziani, R. In *The Chemistry of Cements*; Taylor, H. F. W., Ed.; Academic Press: London and New York, 1964; Vol. 1, p 233.
(25) Whittington, B. I.; Cardile, C. M. *Int. J. Miner. Process.* **1996**, *48*, 21.
(26) Wright, K.; Freer, R.; Catlow, C. R. A. *Phys. Chem. Miner.* **1994**, *20*, 500.
(27) Whittington, B. I.; Fallows, T. M.; Willing, M. J. *Int. J. Miner. Process.* **1997**, *49*, 1.
(28) Gale, J. D. *J. Chem. Soc., Faraday Trans.* **1997**, *93*, 629.
(29) Dick, B. G.; Overhauser, A. W. *Phys. Rev.* **1958**, *112*, 90−103.
(30) Gay, D. H.; Rohl, A. L. *J. Chem. Soc., Faraday Trans.* **1995**, *91*, 925.
(31) Gale, J. D.; Rohl, A. L.; Watling, H. R.; Parkinson, G. M. *J. Phys. Chem. B* **1998**, *102*, 10372.
(32) Cerius^2 Version 4.0; Molecular Simulations Inc.: San Diego, 1999.
(33) Fleming, S. D. Ph.D. Thesis, School of Applied Chemistry; Curtin University of Technology: Perth, 1999.
(34) Barlow, S.; Rohl, A. L.; Shi, S.; Freeman, C. M.; O'Hare, D. *J. Am. Chem. Soc.* **1996**, *118*, 7578.
(35) Tasker, P. W. *J. Phys. C Solid State Phys.* **1979**, *12*, 4977.
(36) Spierings, G. A. C. M.; Stein, H. N. *Colloid Polym. Sci.* **1978**, *256*, 369.